

Solution domains of the Gierer Meinhardt Equations - Parameter studies on the activator inhibitor system

Klaus Räddecke, Rüsselsheim

February 2023

Abstract

The activator inhibitor system of space-temporal differential equations are analyzed, following a formulation given by Gierer and Meinhardt. Several steps were taken by fixed point analysis and numerical experiments.

Bifurcation surfaces in the parameter space were found. Also, the type of the bifurcation could be identified. The analytical findings were compared to numerical simulations. To identify the cause of discrepancies, very detailed analysis was done on the methods.

Then the influence of agent inflow or outflow was analyzed and a complex bifurcation diagram is shown.

Using a stationary but spacially oscillation solution from a numerical experiment, the local transition of the oscillators behavior can be explained.

The equations have then been studied with diffusion in a two- or three dimensional rectangular grid, by varying up to three parameters all in one simulation run, and evaluated using video. Typical behavior of the solution could be visualized.

Introduction

The Gierer Meinhardt equations have been introduced in early 1990 decade, and Meinhardt evaluated solutions suitable to generate patterns observed in sea shells. In his book, most evaluations considered an 1-dimensional domain evolving in time, but he also showed some examples of 2-dimensional solutions. Parameters he used were included in a floppy disk attached to

the book. This work sticks to his nomenclature except for capitalizing the variable names, and no rescaling is done, to directly compare the results for validation.

Extensive use of the machine algebra package sympy was made to analyze the states of the oscillator.

With vastly expanded compute power, the solution domain was expanded to 3-dimensional space.

To get an overview on the possible solutions, some parameters of the equations were mapped to the spacial domain. If the parameter changes of the mapping are small, a good impression of the dynamics in the parameter range can be expected. This was solved in transient and post processed.

Part I

The activator inhibitor oscillator

1 Formulation

In this work, the basic activator-inhibitor system was used with saturation term for autocatalysis of the activator concentration s_a , and a (small) constant source of inhibitor b_b .

$$\frac{\partial}{\partial t} A = s \left(\frac{A^2}{B(1 + s_a A^2)} + b_a \right) - r_a A + D_a \Delta A \quad (1)$$

$$\frac{\partial}{\partial t} B = s A^2 - r_b B + b_b + D_b \Delta B \quad (2)$$

The parameters r_a and r_b are the decay parameters, b_a and b_b are sources and D_a and D_b the diffusion coefficients for the substances A and B respectively.

In the following, the local amplification capability s is set constant. Meinhardt used it to add random perturbations like $1 + \epsilon(x)$, while here I use random perturbations from the initial conditions.

2 The founding oscillator

This part analyses the behavior of the basic dynamical equation, if $D_a = 0$ and $D_b = 0$. Also, the modifying parameters in this section are set $s_a = 0$

and $b_b = 0$. Even using sympy symbolic algebra, fixed points could not be solved for in the cases with saturation.

2.1 Linear stability analysis

Fixed points can be found from the steady state, non-diffusive equations

$$-Ar_a + s \left(\frac{A^2}{B} + b_a \right) = 0$$

$$A^2s - Br_b = 0$$

at $A_f = \frac{b_a s + r_b}{r_a}$ and $B_f = \frac{s(b_a s + r_b)^2}{r_a^2 r_b}$. The eigenvalues are

$$E_1 = \frac{2As - Br_a - Br_b}{2B} - \frac{\sqrt{-8A^3s^2 + 4A^2s^2 - 4ABr_a s + 4ABr_b s + B^2r_a^2 - 2B^2r_a r_b + B^2r_b^2}}{2B}$$

and

$$E_2 = \frac{2As - Br_a - Br_b}{2B} + \frac{\sqrt{-8A^3s^2 + 4A^2s^2 - 4ABr_a s + 4ABr_b s + B^2r_a^2 - 2B^2r_a r_b + B^2r_b^2}}{2B}$$

Substituting the fixed point, and re-arranging terms this is

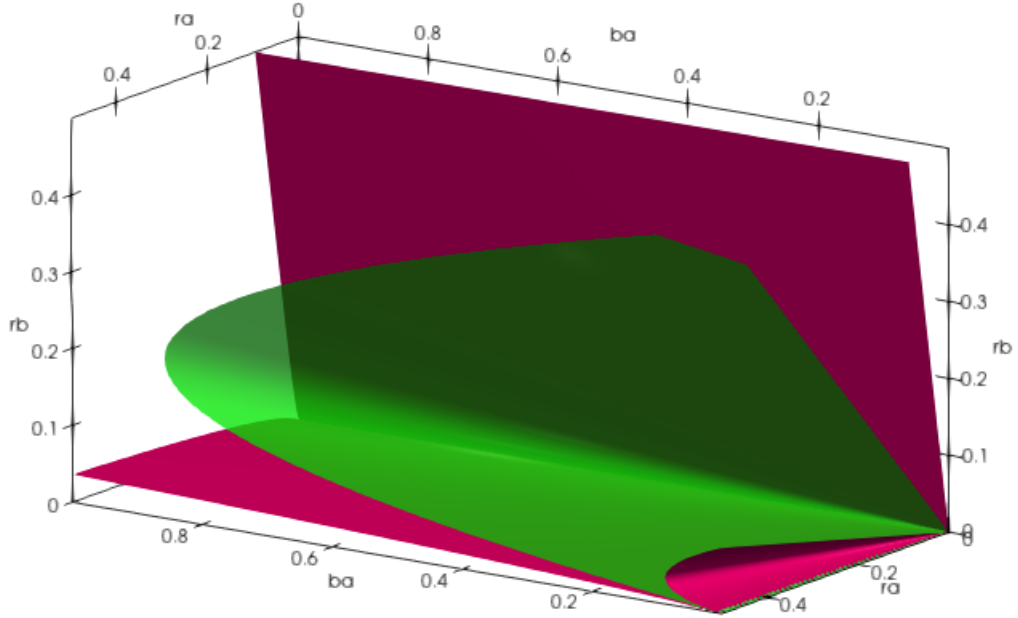
$$E_b := \frac{-b_a r_a s - b_a r_b s + r_a r_b - r_b^2}{2(b_a s + r_b)}$$

$$E_q^2 := \frac{b_a^2 r_a^2 s^2 - 2b_a^2 r_a r_b s^2 + b_a^2 r_b^2 s^2 - 2b_a r_a^2 r_b s - 8b_a r_a r_b^2 s + 2b_a r_b^3 s + r_a^2 r_b^2 - 6r_a r_b^3 + r_b^4}{4(b_a^2 s^2 + 2b_a r_b s + r_b^2)}$$

Instability occurs at

$$\begin{cases} E_b = 0 & E_q^2 \leq 0 \\ E_b + E_q = 0 & E_q^2 > 0 \end{cases}$$

To visualize the bifurcation scenario, for $s = 0.1$ the solutions to this were numerically evaluated over the parameter range and in this voxel field, the surface to match the condition was found using a marching cubes algorithm. Resolution chosen were $1.e9$ evaluations. Also in the diagram, the solution to $E_q^2 = 0$ was searched, to visualize where a Hopf bifurcation would turn into a saddle-node bifurcation.

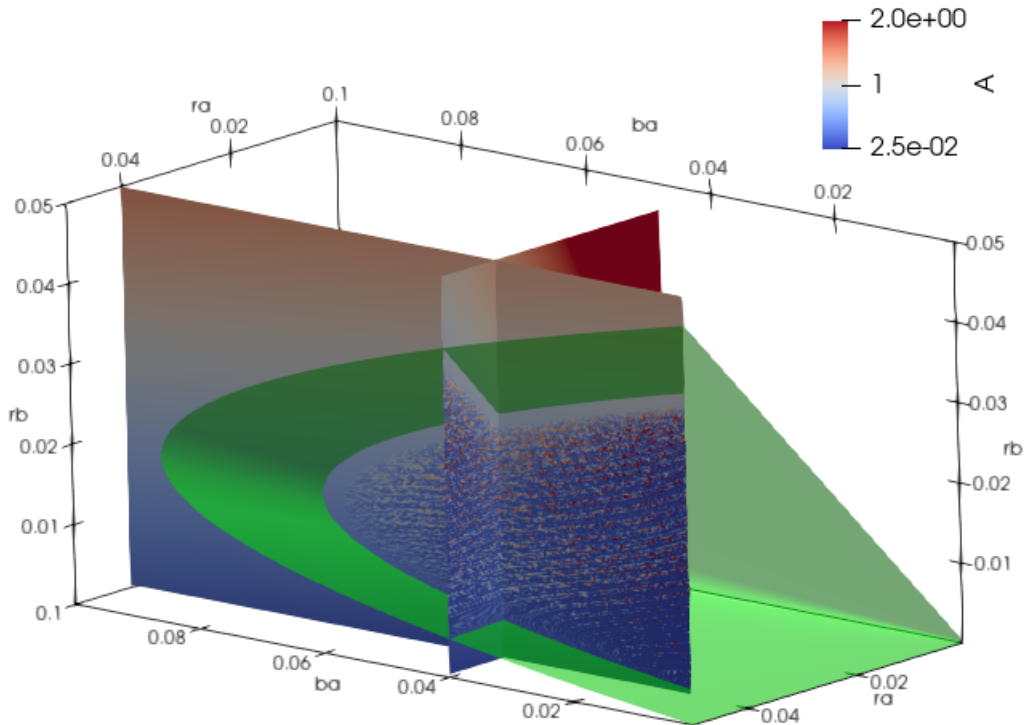


This plot shows ANALYTICAL BIFURCATION FACES in the parameter space. The green surface is where the instability occurs, and the red surface is the transition of the eigenvalue type. The surfaces do only intersect in the r_a axis. Any instability for $b_a > 0$ is oscillatory.

2.2 Numerical stability analysis

For a numerical confirmation, I ran two 2d simulations (see below), where diffusion was switched off so that with every point in the discretized rectangle, the pair of equations are autonomous.

To do this, I used the OpenFOAM software, to write a solver for the Meinhardt equations. Using this, the full framework for 3d operations is available, from creation of computational meshes, managing parameters, solving in parallel, and post processing in Paraview. Here, two 2d simulations involving $4.7e6$ oscillators add two numerical result planes at $b_a = 0.04$ and $r_a = 0.04$ into the picture:



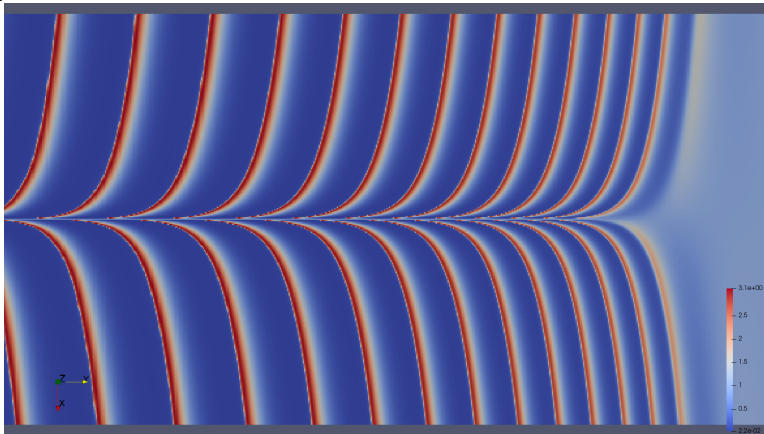
In this OVERLAY PLOT most of the parameter space within the fold of the green surface is also numerically unstable. Close to the bifurcation, however, the numerical solution is stable in contrast to the analytical prediction. This mismatch provokes a more close investigation.

So how to resolve this discrepancy? The first topic I look at is the numerics. Do the fixed points hold over time even under rounding errors? Then, I tested the sensitivity of the solver – even without diffusivity – to be affected by high dynamics across the parameter space. The second topic is to find analytical approximate solutions, either to give hints on the parameter sensitivity as well on the frequency and phase relationships. Besides the eigenvalue analysis, a harmonic balance method was tried to get amplitudes near the bifurcation. Following up, another attempt to find amplitudes near the bifurcations was attempted.

2.3 Numerical investigations

OpenFoam, as a well respected package, might be challenged by such a type of equation, so I explored some aspects. The first aspect to look at is the stability of the solver if initialized on an unstable fixed point, and how systematic deviations affect the oscillations that will occur. There are no diffusion terms involved.

A small offset to $A(t = 0)$ has been added to the initial conditions set by the fixed point analysis outlined above. Pattern structures therein are still due to initial conditions and the asymmetrical character of the equations. This comes clear when looking at a systematically varied initial condition in a 2d simulation varying r_b on one axis, and an initial offset to the fixed point of A in perpendicular in the following plot with 1440x315 oscillators are run in parallel:

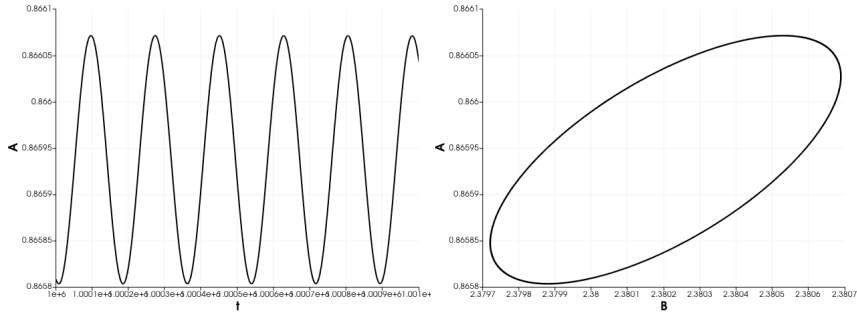


In this FISHBONES like image, r_b is varied horizontally. The center horizontal line is the unstable fixed point, and vertically spans a \pm offset on the initial condition to A . $s = 0.1$, $r_a = 0.04\bar{6}$, $b_a = 0.01$. This is the situation after 50,000 time steps. The waves move to the left. The initial offset determines the timing of the oscillations. Temporal solver method used was “Euler”. This behavior testifies, that the numerics does keep the unstable fixed point (for a while). Emergence of that pattern is appended in a video¹. The very right area in the image covers the vanishing amplitudes towards a stable solution. Also here, the onset of oscillations does not match the analytical result.

It was also noted, that for small values of b_a , the amplitudes get very high, and so there is a large dynamical range in the mesh fields. With that, error correction mechanisms in the solver start to modify solution convergence, and, although there is no diffusion from the equations, the solver itself does some global damping. Further tests showed, that the bifurcation border stabilizes if $b_a > 0.01$ in the simulation domain.

The time series very close to the bifurcation point looks very harmonic:

¹2d/fishbones.mp4



The OSCILLATION shown as time series and as a Lissajous plot is at $s = 0.1$, $b_a = 0.03134$, $r_a = 0.04$, $r_b = 0.031499$. It could be a good idea to try the method of harmonic balance to get the limit cycle amplitudes close to the bifurcation for comparison to the numerical results.

2.4 Analytical investigations

To try a harmonic ansatz on the oscillator we consider

$$\frac{d}{dt}A = s \left(\frac{A^2}{B} + b_a \right) - r_a A \quad (3)$$

$$\frac{d}{dt}B = sA^2 - r_b B \quad (4)$$

2.4.1 The first ansatz

Using (3) and (4) directly, we insert the ansatz

$$\begin{aligned} A &= A_0 + A_1 e^{i\omega t} \\ B &= B_0 + B_1 e^{i\omega(t+\tau)} \end{aligned}$$

τ needs to model the lagging of the inhibitor behind activator concentration. It comes straight forward to identify $A_0 = A_f$ and $B_0 = B_f$ from above. The trick now is to calculate Fourier coefficients which then will be required to be zero.

Substituting the ansatz and the fixed point into (3) and (4), we write the integrals for the first order harmonic:

$$\begin{aligned}
0 &= \int_0^{\frac{2\pi}{\omega}} \left(-A_1^2 s e^{i\omega t} + iA_1 B_1 \omega e^{i\omega t} e^{i\omega\tau} + A_1 B_1 r_a e^{i\omega t} e^{i\omega\tau} \right) dt \\
&+ \int_0^{\frac{2\pi}{\omega}} \left(\frac{iA_1 b_a^2 \omega s^3}{r_a^2 r_b} + \frac{A_1 b_a^2 s^3}{r_a r_b} + \frac{2iA_1 b_a \omega s^2}{r_a^2} + \frac{iA_1 \omega r_b s}{r_a^2} - \frac{A_1 r_b s}{r_a} + B_1 r_b e^{i\omega\tau} \right) dt
\end{aligned}$$

and

$$0 = \int_0^{\frac{2\pi}{\omega}} \left(-A_1^2 s e^{i\omega t} - \frac{2A_1 b_a s^2}{r_a} - \frac{2A_1 r_b s}{r_a} + iB_1 \omega e^{i\omega\tau} + B_1 r_b e^{i\omega\tau} \right) dt$$

These evaluate to the set of equations

$$0 = \frac{iA_1 b_a^2 \omega r_a^4 r_b s^3 + A_1 b_a^2 r_a^5 r_b s^3 + 2iA_1 b_a \omega r_a^4 r_b^2 s^2 + iA_1 \omega r_a^4 r_b^3 s - A_1 r_a^5 r_b^3 s + B_1 r_a^6 r_b^3 e^{i\omega\tau}}{r_a^6 r_b^2} \quad (5)$$

and

$$0 = \frac{-2A_1 b_a s^2 - 2A_1 r_b s + iB_1 \omega r_a e^{i\omega\tau} + B_1 r_a r_b e^{i\omega\tau}}{r_a} \quad (6)$$

Solving (6) for A_1 gives a proportional dependency on B_1 . When substituting into (5), $A_1 > 0$ cancels out, we see one complex equation for ω and τ . First solving the real part

$$0 = -\frac{\omega b_a^2 s^3 \sin(\omega\tau)}{2b_a r_b s^2 + 2r_b^2 s} + \frac{\omega r_b s \sin(\omega\tau)}{2b_a s^2 + 2r_b s} + \frac{b_a^2 s^3 \cos(\omega\tau)}{2b_a s^2 + 2r_b s} - \frac{r_b^2 s \cos(\omega\tau)}{2b_a s^2 + 2r_b s} + r_b \cos(\omega\tau)$$

of it for τ , we find two solutions as

$$\tau_{1/2} = -\frac{2}{\omega} \operatorname{atan} \left(\frac{\omega (b_a s - r_b) \pm \sqrt{b_a^2 \omega^2 s^2 + b_a^2 r_b^2 s^2 - 2b_a \omega^2 r_b s + 2b_a r_b^3 s + \omega^2 r_b^2 + r_b^4}}{r_b (b_a s + r_b)} \right)$$

Substituting this into the imaginary part of the complex equation leaves us with:

$$\begin{aligned}
0 &= -\frac{\omega^2 b_a^2 s^3 \sin(\omega\tau)}{2b_a r_a r_b s^2 + 2r_a r_b^2 s} - \frac{2\omega^2 b_a s^2 \sin(\omega\tau)}{2b_a r_a s^2 + 2r_a r_b s} - \frac{\omega^2 r_b s \sin(\omega\tau)}{2b_a r_a s^2 + 2r_a r_b s} \\
&+ \frac{\omega b_a^2 s^3 \cos(\omega\tau)}{2b_a r_a s^2 + 2r_a r_b s} + \frac{2\omega b_a r_b s^2 \cos(\omega\tau)}{2b_a r_a s^2 + 2r_a r_b s} + \frac{\omega r_b^2 s \cos(\omega\tau)}{2b_a r_a s^2 + 2r_a r_b s} + r_b \sin(\omega\tau)
\end{aligned}$$

To solve this for ω is unfeasible analytically, and so it was done numerically for the parameters we wanted to investigate near the bifurcation border. It turns out, that both of $\tau_{1/2}$ return the same values for ω . The result is shown below.

But, unfortunately, we do not have amplitudes. I will spoiler it: Including the next harmonic leaves the same problem.

2.4.2 The second ansatz

This way, before we make an ansatz, we transform (3) and (4) into a differential equation of second order around the fixed point: $A = \tilde{A} + A_f$ and $B = \tilde{B} + B_f$. With this, (3) can be solved for \tilde{B} , and then substituted into (4) which gives, expanded:

$$\frac{d^2}{dt^2}\tilde{A} = \frac{k_0 \frac{d}{dt}\tilde{A} + k_1 \left(\frac{d}{dt}\tilde{A}\right)^2 + k_2 \tilde{A} + k_3 \tilde{A} \frac{d}{dt}\tilde{A} + k_4 \tilde{A} \left(\frac{d}{dt}\tilde{A}\right)^2 + k_5 \tilde{A}^2 + k_6 \tilde{A}^2 \frac{d}{dt}\tilde{A} + k_7 \tilde{A}^3}{b_a s + r_a \tilde{A} + r_b}$$

with coefficients defined as:

$$k_0 := -b_a r_a s - b_a r_b s + r_a r_b - r_b^2, \quad k_1 := -b_a s + 2r_a - r_b, \quad k_2 := -b_a r_a r_b s - r_a r_b^2, \\ k_3 := -2b_a r_a s + r_a^2 - 3r_a r_b, \quad k_4 := -r_a, \quad k_5 := -b_a r_a^2 s - 2r_a^2 r_b, \quad k_6 := -2r_a^2, \\ k_7 := -r_a^3.$$

In contrast to the first ansatz, there is no τ required, so the ansatz $\tilde{A} = A_1 \sin(\omega t)$ is sufficient. Substituting the ansatz and expanding the differentials returns another equation too long to print.

As this equation is nonlinear by a divisor, if substituting a harmonic ansatz, no further progress in analysis is possible. But, as \tilde{A} is small, the denominator can be expanded through Taylor's rule. The denominator is approximated by

$$\frac{1}{A_1 r_a \sin(\omega t) + b_a s + r_b} \approx \frac{A_1^2 r_a^2 \sin^2(\omega t)}{(b_a s + r_b)^3} - \frac{A_1 r_a \sin(\omega t)}{(b_a s + r_b)^2} + \frac{1}{b_a s + r_b}$$

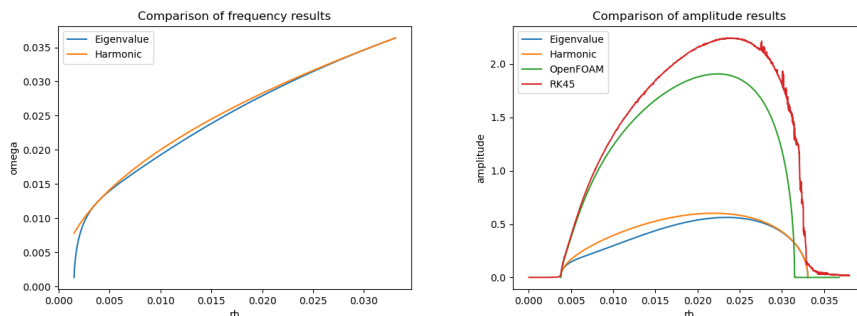
With trigonometric formulas the equation can be further expanded. Integration over one oscillation period of this beast is quick, and solving for A_1 returns a formula for two amplitudes having opposite signs:

$$A_1 = (\pm) \frac{2 \sqrt{\frac{\omega^2 b_a s - 2\omega^2 r_a + \omega^2 r_b + b_a r_a^2 s + r_a^2 r_b}{2\omega^2 - 3r_a r_b}} (b_a s + r_b)}{r_a^{\frac{3}{2}}} \quad (7)$$

So, here we get an amplitude, but no frequency.

2.4.3 Combining the ansatzes

So we have frequencies from the eigenvalue analysis and from the harmonic balance on the first ansatz. As it is to be discussed, which of them is better suited to approximate ω in (7), I tried both of them, first to compare the curves $\omega(r_b)$ and $A_1(r_b)$ at $s = 0.1$, $b_a = 0.03134$ and $r_a = 0.04$. For the amplitude diagram, numerical results are also included.



In a wide range, the frequency curves match quite well, except for the low end, but the match is nearly perfect in the r_b range where we were interested in $[0.03 \dots 0.035]$. Using these frequencies for evaluation of (7), the amplitudes also match, and show a drastic decline when approaching the bifurcation. In the amplitude diagram, the same parameters were used to run 1000 oscillators using OpenFoam, and measure the resultant amplitudes. And as a third approach, I used a Runge-Kutta 4th order (RK45) to run the same. Keep in mind that the analytical amplitudes are valid for small amplitudes only. Unfortunately, there is no explanation still about the discrepancy between analysis and numerics for the upper r_b bound of zero crossings: the analytical results are consistent with each other, but the OpenFoam oscillations clearly fade at lower values of r_b . And with the Runge-Kutta method, although it looks like the bifurcation point would match the analytical approach, the solver produces stable oscillatory solutions of small amplitudes at parameters which would be expected to be stable at the fixed point. For small values of r_b , the bifurcation point is matched by all methods.

This makes it visible, that the numerical methods do create different results, and have different problems on accuracy.

Part II

Spacial considerations

3 Neighbor sources

As with significant diffusion, stable structures emerge, which, from an oscillator perspective, means changes to b_a and b_b source terms, such that a fixed point is reached. So let us look for such fixed points.

To get an approach to neighbor cell coupling, the first step is to check the influence of an inhibitor source, and to see how fixed points will change due to source or sink like it would be in a stabilized structure pattern. So we use equation (3) and add the source b_b to equation (4):

$$\frac{d}{dt}B = sA^2 - r_bB + b_b$$

For $b_b \neq 0$ there are three roots to this system of equations. Here we see, how b_b affects the fixed point A_f from above.

$$A_{f1} = -\frac{k_1}{3k_2} - \frac{k_2}{3} - k_3$$

$$A_{f2} = -\frac{k_1}{3k_2 \left(-\frac{1}{2} - \frac{\sqrt{3}i}{2}\right)} - \frac{k_2 \left(-\frac{1}{2} - \frac{\sqrt{3}i}{2}\right)}{3} - k_3$$

$$A_{f3} = -\frac{k_1}{3k_2 \left(-\frac{1}{2} + \frac{\sqrt{3}i}{2}\right)} - \frac{k_2 \left(-\frac{1}{2} + \frac{\sqrt{3}i}{2}\right)}{3} - k_3$$

$$B_{f1} = -\frac{s(k_1 + k_2(k_2 + 3k_3))^2}{3k_2 \cdot (3b_a k_2 s + r_a(k_1 + k_2(k_2 + 3k_3)))}$$

$$B_{f2} = -\frac{s \left(k_1 + k_2 \cdot \left(\frac{1}{2} + \frac{\sqrt{3}i}{2}\right)\right) \left(k_2 \cdot \left(\frac{1}{2} + \frac{\sqrt{3}i}{2}\right) - 3k_3\right)^2}{3k_2 \cdot \left(\frac{1}{2} + \frac{\sqrt{3}i}{2}\right) \left(3b_a k_2 s \left(\frac{1}{2} + \frac{\sqrt{3}i}{2}\right) - r_a \left(k_1 - k_2 \cdot \left(\frac{1}{2} + \frac{\sqrt{3}i}{2}\right) \left(-k_2 \cdot \left(\frac{1}{2} + \frac{\sqrt{3}i}{2}\right) + 3k_3\right)\right)}$$

$$B_{f3} = -\frac{s \left(k_1 + k_2 \left(-\frac{1}{2} + \frac{\sqrt{3}i}{2}\right)\right) \left(k_2 \left(-\frac{1}{2} + \frac{\sqrt{3}i}{2}\right) + 3k_3\right)^2}{3k_2 \left(-\frac{1}{2} + \frac{\sqrt{3}i}{2}\right) \left(3b_a k_2 s \left(-\frac{1}{2} + \frac{\sqrt{3}i}{2}\right) + r_a \left(k_1 + k_2 \left(-\frac{1}{2} + \frac{\sqrt{3}i}{2}\right) \left(k_2 \left(-\frac{1}{2} + \frac{\sqrt{3}i}{2}\right) + 3k_3\right)\right)}$$

where the coefficients are given by

$$\begin{aligned}
k_1 &:= A_f^2 - \frac{3b_b}{s} \\
k_2 &:= \sqrt[3]{-A_f^3 + \frac{9A_fb_b}{2s} - \frac{27b_ab_b}{2r_a} + \frac{\sqrt{-4\left(A_f^2 - \frac{3b_b}{s}\right)^3 + \left(-2A_f^3 + \frac{9A_fb_b}{s} - \frac{27b_ab_b}{r_a}\right)^2}}{2}} \\
k_3 &:= -\frac{A_f}{3}
\end{aligned}$$

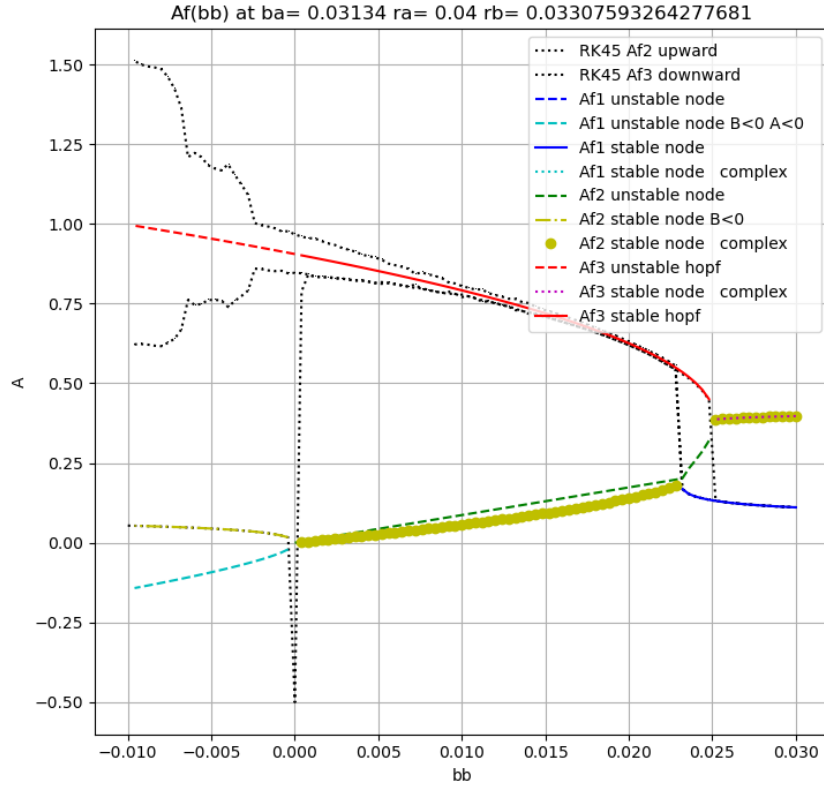
Then, as in above's linear stability analysis, the eigenvalues can be calculated at the fixed points, for each of the A_f 's.

$$e_{\pm} = r \pm \sqrt{q}$$

where

$$\begin{aligned}
r &= \frac{2As - Br_a - Br_b}{2B} \tag{10} \\
q &= \frac{-8A^3s^2 + 4A^2s^2 - 4ABr_as + 4ABr_bs + B^2r_a^2 - 2B^2r_ar_b + B^2r_b^2}{4B^2} \tag{11}
\end{aligned}$$

With this, a classification of the fixed points can be done: if $q < 0$, then $r = 0$ determines bifurcation, while if $q \geq 0$, $r + \sqrt{q}$ is the stability criterion. To insert the fixed points $(A_{f1}, B_{f1}), (A_{f2}, B_{f2}), (A_{f3}, B_{f3})$ analytically to the eigenvalue formulas requires careful numerical evaluation thereafter. Additional classification is to check both physical concentrations $A, B > 0$, and that the fixed point is in \mathfrak{R} .



This BIFURCATION DIAGRAM shows the A values of the three fixed points in their dependency on b_b . At $b_b = 0$, the system is at the upper bifurcation point in the amplitude graph in section 2.4.3. The fixed point A_{f_3} bifurcates from its center type stability at $b_b = 0$ to stable ($b_b > 0$) and unstable ($b_b < 0$) foci. For $b_b > 0.025$ this root becomes conjugate complex with A_{f_2} , and is not a physical fixed point anymore. Negative b_b leave the system with an unstable focus. This is surrounded by a limit cycle; the amplitudes are indicated by the dotted black RK45 lines. As we have seen in the previous section 2.4.3 with RK45, that solver tends to be unstable with the stable focus, and the dashed lines just tighten around, not merge to the A_{f_3} curve.

While with A_{f_2} an additional stable node exists (dash-dot yellow), where the activator concentration is very low, the inhibitor concentration $B_{f_2} < 0$, and so this is also no physical solution. Anyway, the numerical solution confirmed that analytical finding (dotted line). Note, that $A_{f_1} < 0$ and is no concentration. A_{f_1} and A_{f_2} become conjugate complex (yellow dots) for a range $b_b \in [0 \dots 0.023]$, which excludes them from realization in the system. Numerical solution does not follow that path, but the solution jumps up

to the stable focus of A_{f3} . Note, that the numerical solution at $b_b = 0$ is significantly off (and also clipped in this plot to $A = -0.05$) as this is a critical point for the A_{f1} and A_{f2} to merge into a conjugate complex pair which creates numerical dispair for $b_b \in [-10^{-100} \dots 0]$. Further up in $b_b \in [0.023 \dots 0.025]$, the stable focus of A_{f3} and the stable node of A_{f1} coexist, and with a parameter sweep up and down around that range, hystheresis is observed. For $b_b > 0.025$, the only physical solution remaining is the node of A_{f1} .

4 Including diffusion

In this work, numerical experiments for the diffusive and dynamical equations (1) and (2) were done. As Meinhardt appended a floppy disk in his book, his results displayed in his figures 2.11 and 2.12 could be qualitatively reproduced. Also, although from the previous numerical investigations there remains a systematical difference in parts of the parameter space, OpenFoam still provided the code base for the following.

With diffusive coupling, the mesh grid size becomes a significant parameter for the validity of solutions: The mesh must be fine enough to resolve the structure gradients. Any change to the diffusion coefficients $D_a > 0$ and $D_b > 0$ can be rescaled from equations (1) and (2) into length scale. Knowing this, it is clear, that the interesting limit of vanishing diffusion cannot be explored in the limit of small diffusion, as the grid length scale must change accordingly to resolve structures properly. Also, the implications in generalization from 2d to 3d are touched. This will be covered in the first subsection.

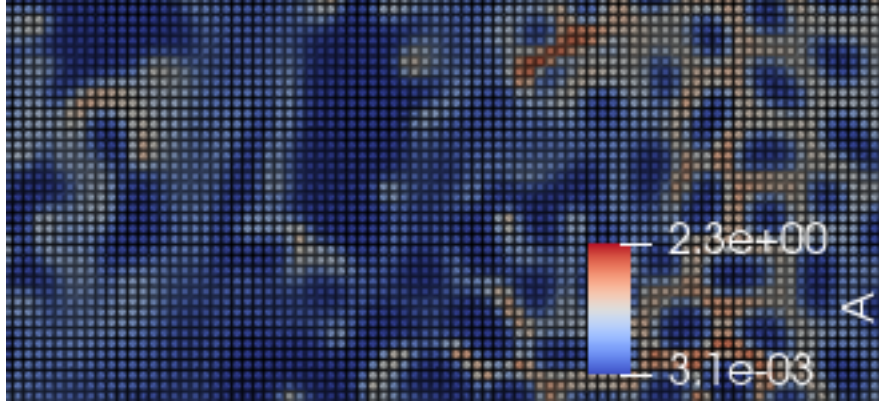
Throughout this chapter, the parameters are varied spacially with low gradients. This way, both the spacial structure generation, as well as the parameter dependence of this can be represented in one glance. To check on the quality of such an approach, I compared a planar section of a 3d simulation with a 2d simulation and found good agreement. This is the second subsection.

Parameters used in this section are, if not otherwise noted, fixed to $s = 0.1$, $b_b = 0$, $s_a = 0.0$. Generally here I use $D_b > D_a$, a known condition for pattern formation.

4.1 Mesh grid

For a typical parameter situation, here is an image showing activator structures plus the grid at $r_b \in [0.003 \dots 0.00314]$ vertically, $D_b \in [0.036 \dots 0.044]$

horizontally:

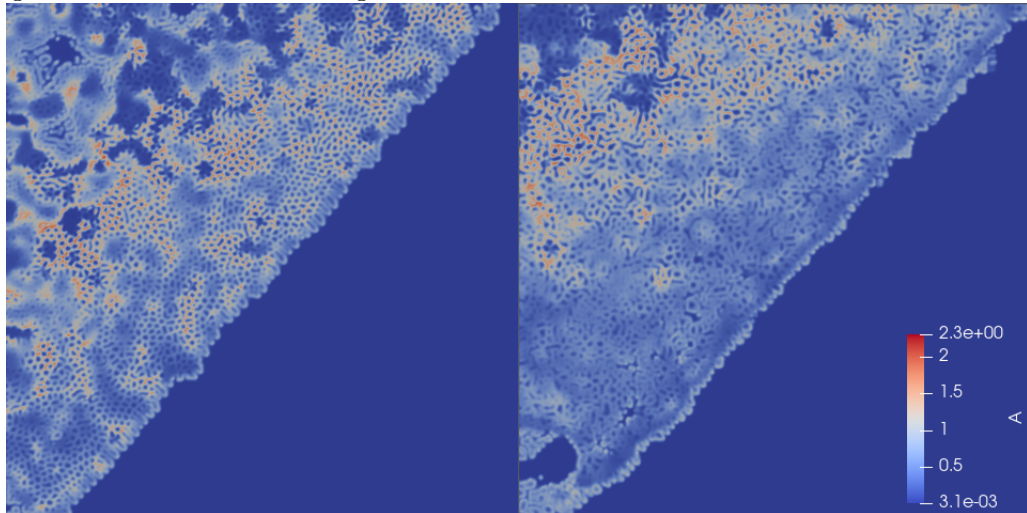


This MESH GRID plot shows about 7 computational cells spanning the typical structure length. So for the given grid edge length of 1, D_a and D_b are kept larger than 0.01.

4.2 Parameter to space consistency

A 3d simulation was run on a 480 x 480 x 480 cell grid for 8500 time steps. So the solution is not fully stabilized with its static and dynamical structures. Still the main features can be watched stabilizing in videos. This simulation spanned $b_a \in [0.002 \dots 0.026]$, $b_b \in [0 \dots 0.00015]$ and $r_b \in [0.01 \dots 0.045]$.

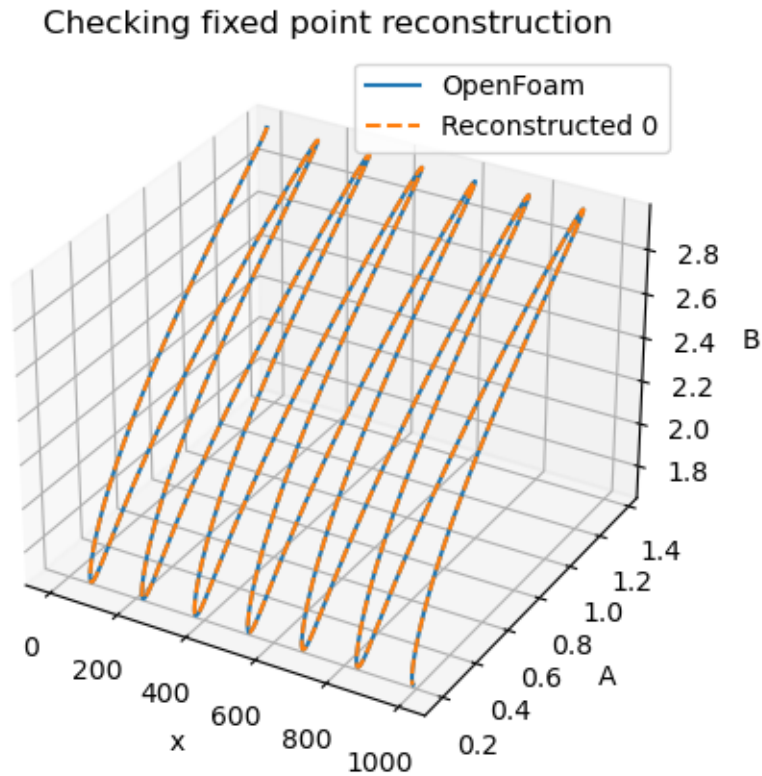
To check whether a 2d simulation has the same results, $r_a = 0.03$ the images and use the same ranges as the 3d case.



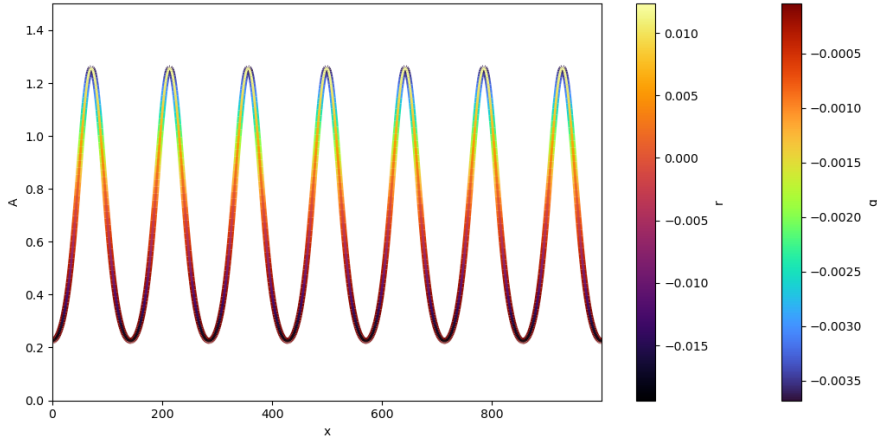
2d (left) versus 3d (right). Both cases are still evolving, especially the 3d case which was limited to only 8500 time steps. In both cases, the structure front still expands towards the lower right corner.

4.3 Oscillator perspective on diffusion

If a spacial simulation is available, the diffusion terms in (1) and (2) can be calculated from the solution. With this reconstructed data, we can look at the oscillator state using the classification described in paragraph 3. Now look at a situation, where the solution shows stable, dynamical structures. I pick one from the intersection of the two simulated planes introduced in section 2.2 at $r_b = 0.025$ and diffusion coefficients of $D_a = 5$ and $D_b = 50$, which gives a very smooth spacial wave along a oscillator chain. From OpenFoam, we get $A(x)$ and $B(x)$, and from that, $\frac{\partial^2 A}{\partial x^2}$ and $\frac{\partial^2 B}{\partial x^2}$ can be calculated. With the known parameters, the concentrations A and B can be calculated from the roots (8) and (9). As long as $|\Im(A_{f3})| > 0$, $\Re(A_{f1})$, else A_{f3} will be used, which is in \Re . Here is a comparison of the reconstruction versus OpenFoam in a phase space:



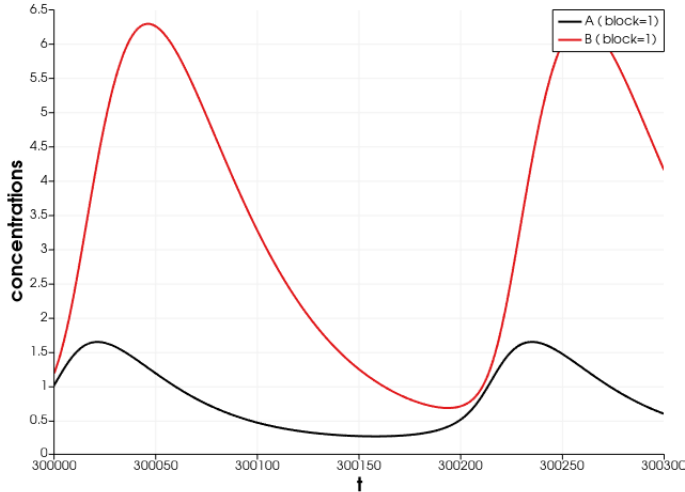
This can then be used to check the status of the stationary oscillator. The same spacial oscillation can now be colored by the eigenvalues of the fixed point, the oscillators are:



The A amplitude is center colored by the real part r (or $r + \sqrt{q}$ if $q > 0$) and surrounded by the discriminant q of the eigenvalues in formulas (10) and (11) respectively. Oscillation frequencies slow down on low activity, as $q \approx \omega^2$ if it is negative. While r indicates stability for lower values of A , at high values the system becomes unstable. q indicates only focal type.

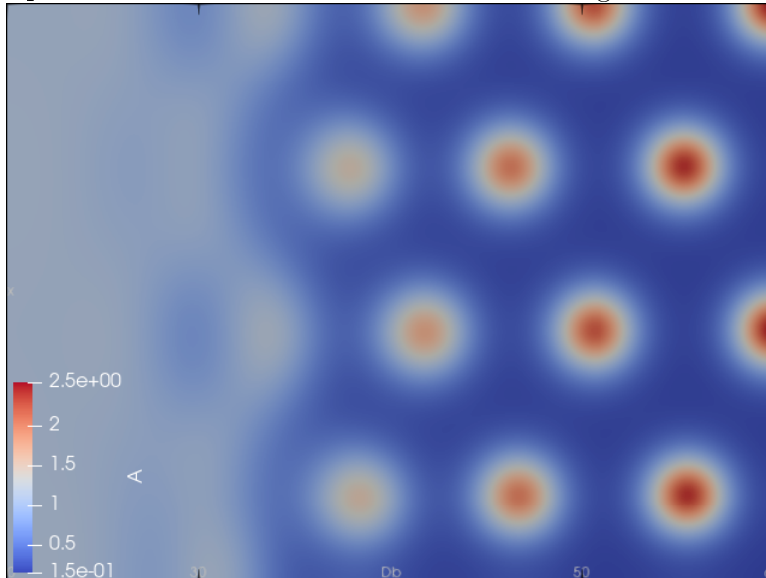
4.4 Diffusion effect

In 4.3 we analyzed a steady state solution at a parameter set, which would oscillate autonomously if a cell would be decoupled. This was with a ratio of the diffusion coefficients of $D_a/D_b = 5/50$ where the spacial structure freezes. With lower ratio of $D_a/D_b = 5/20$, the solution is, in contrast, a synchronized oscillation:



So, using the slowly varying parameters method is used to display the transition from homogeneous oscillation to steady state patterns. A 2d sim-

ulation is varying D_b between those parameter points, while giving room for the spacial structures on a x coordinate. This gives the following snapshot:



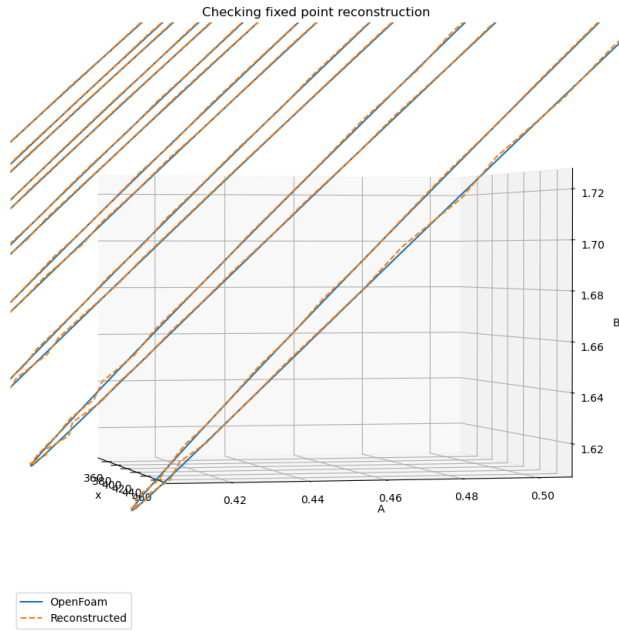
On the left, what appears to be homogeneous, does oscillate in sync. The dots to the right are localized. Around $D_b \simeq 30$, the structures start to show up; although the minima and maxima stay at these positions, they still are like swimming on the oscillation as to the left. The dots up to $D_b \simeq 35$ also still oscillate, but the surrounding low concentration areas become constant.

Running a series of 1d simulations gives a sharper distinction between those behavioral regimes, and close to that bifurcation point, in a still slightly oscillating but structured situation at $D_b = 38$, we first need to get some estimation for the driving laplace calculation from the solution - as it oscillates, it has not the values as in the unstable fixed point. Now close to the fading of instability, oscillation amplitudes are small and nearly harmonic (see 2.3). So the averaging ansatz for the external driving fluxes to apply the method layed out in paragraph 4.3 is

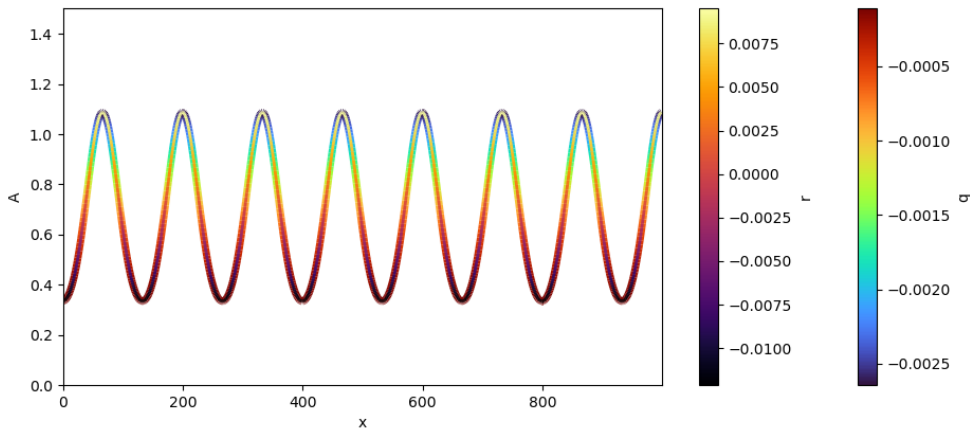
$$s\bar{b}_a \approx sb_a + D_a \frac{\omega}{2\pi} \int_0^{\frac{2\pi}{\omega}} \frac{\partial^2 A}{\partial x^2} dt \quad (12)$$

$$\bar{b}_b \approx D_b \frac{\omega}{2\pi} \int_0^{\frac{2\pi}{\omega}} \frac{\partial^2 B}{\partial x^2} dt \quad (13)$$

At $D_b = 38$, the reconstructed solution is still close to the time averaged solution:



With this accepted, the classified structure looks like:



In contrast to the analysis of the situation at $D_b = 50$, here we see a switch in stability ($r = 0$), where the oscillators states become unstable foci at high amplitudes A and stable focus at low amplitudes A . This explains the oscillating spots in a seemingly constant inhibited area. Very small disturbances get across the weak stable foci, which is sufficient to synchronize spot oscillations. Note, that, although q is negative, it comes very close to 0 where, at low A , stable attractors were also found at $D_b = 50$ in OpenFoam.

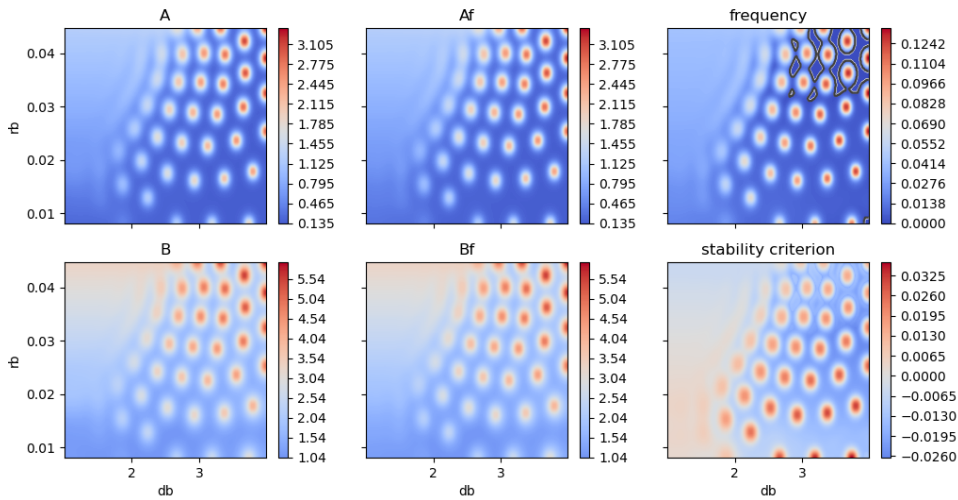
Part III

Spatial pattern dynamics

As mentioned, mapping slowly varying parameters to space, it is possible to simulate millions of oscillators “in parallel” with OpenFoam CFD software. This provides a convenient way to oversee a great range of dynamics in one plot. Notice, that in these studies, the diffusion is selected much smaller, so that the structures again match the mesh study in paragraph 4.1. In this part, some studies are reviewed.

5 Inhibitor decay and diffusion

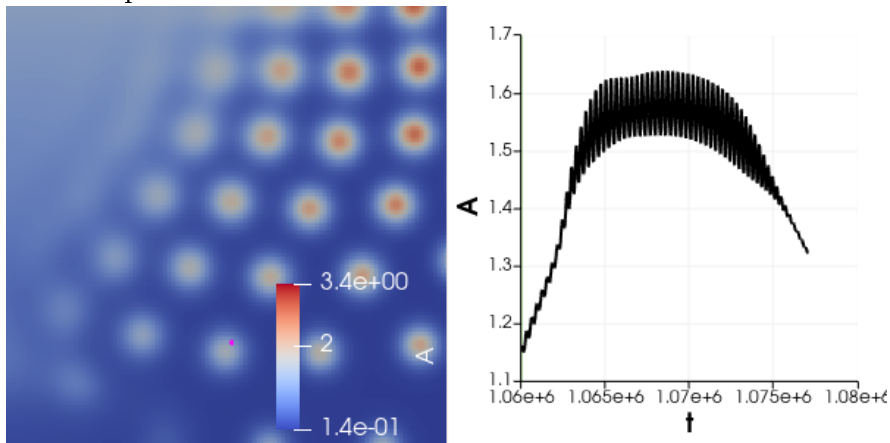
In the following 2d analysis, the control parameters are $r_b \in [0.008 \dots 0.045]$ and $D_b \in [1 \dots 4]$. Fixed parameters were $r_a = 0.04$, $b_a = 0.04$, $b_b = 0$, $D_a = 0.03$ and $s = 0.1$. The transient solution regimes develop quite slowly due to slow changes imposed by the diffusion, starting from an initial condition scattered close to the fixed point. Anyway, after long time, the parameter ranges leading to different solution behavior stabilize. Here is the situation in a 294x196 grid:



The left column of these plots shows the solution of A and B at time step 1077000, the middle column shows the fixed points reconstructed from the Laplacian of the solution, and the right column shows the frequency and the stability criterion as defined in section 3. From that, we see that the centers of the spots are in unstable, oscillating mode, while the separating area is

of stable character with very low frequency, and also a small region of node attractors exist in the higher D_b and r_b range, marked in the frequency plot.

At low $r_b = 0.01$ and low $D_b = 1.5$, the system exhibits oscillatory behavior with a period of approximately 305 time steps or $\omega \sim 0.02$. Oscillations continue to exist between the spots, and generate background waves propagating through between the spots up to approximately $D_b \approx 3$. Here we see an example of a still moving spot close to the low D_b oscillatory region after $1e6$ time steps to relax from the initial transient:



The violet marked cell at $r_b = 0.017$ and $D_b = 2.13$ in the 2d solution image is used to monitor 8500 time steps and plot them over time. During that time, the spot moves towards the upper right, so that the marked cell is finally on the opposite side of the spot. As expected from the previous analysis using the stability criterion, oscillation amplitudes are higher in the center of the spot as in between.

Anyway, in oscillating regions, the solution is not at the oscillators fixed point and the reconstruction comes with errors. A method to get a better approximation of the fixed point of the solution can be to use time averaged simulation results, while amplitudes are small and nearly harmonic as in section 2.3.

6 Parameter studies 2d

Several 2d numerical parameter study simulations were done on a 1920×1080 grid. The images are all colored by A and clipped to the range $[0 \dots 2]$. This tables lists the studies, referring each to a set of base parameters defined thereafter. The first parameter range extends vertically, the second horizontally.

File	Parameter ranges	Base
BA_DB	$b_a \in [0.002 \dots 0.04], D_b \in [0.01 \dots 0.1]$	1
RA_RB	$r_a \in [0.0005 \dots 0.05],$ $r_b \in [0.0005 \dots 0.05]$	4
RB_BA	$r_b \in [0.01 \dots 0.045],$ $b_a \in [0.002 \dots 0.04]$	1
RB_S	$r_b \in [0.01 \dots 0.045],$ $s \in [0.01 \dots 0.1]$	1
RB_SA	$r_b \in [0.01 \dots 0.045],$ $s_a \in [0 \dots 0.2]$	1
RB_DB	$r_b \in [0.01 \dots 0.045],$ $D_b \in [0.05 \dots 0.4]$	2
S_DB	$s \in [0.01 \dots 0.1],$ $D_b \in [0.01 \dots 0.1]$	1
RB_DADB	$r_b \in [0.01 \dots 0.045],$ $D_a \in [0 \dots 0.1], D_b = 8D_a$	1

The RB_DADB study varied the diffusion parameters in constant relation, corresponding to rescaling the length in the equations 1 and 2. Also in this case, diffusion was distributed on the X-axis in the third power $D_x \sim (x/857)^3$ in a 857x500 grid for better visibility.

The base parameter sets are defined as follows:

Base	b_a	b_b	r_a	r_b	s	s_a	D_a	D_b
1	0.01	0	0.046	0.03	0.01	0.1	0.01	0.04
2	0.01	0	0.046	0.03	0.01	0.1	0.04	0.2
4	0.04	0	0.04	0.03	0.1	0	0	0

The images and videos are in the appendix file, 2d subfolder.

7 Parameter studies 3d

Three 3d numerical parameter simulations were done. Because on computational limitations, the videos below show the development of the transient, although the situations shown are close to the final states. They are documented as mp4 video files as follows:

Video	Parameters	Description
bubbleImpressions	r_b, D_b, b_b	Camera flight around the 480x480x480 voxel cube. Iso-surfaces @ $A = 0.8$, colored by B . Boundary colored by A .
coastaledge	r_b, D_b, b_b	See how flat the cut-off by b_b is. Besides the wall, the large waves approach the wall, in the far background, instabilities at very low r_b are visible.
coast	r_b, D_b, b_b	View on the backside of the wall, where the the large waves approach.
layers2	r_b, D_b, b_b	Bubbles for lower r_b values, viewed from the low b_b side. As the system destabilizes for D_b values close to D_a , the amplitudes of concentration can become very high, and so some red bubbles mix into the view. This video also displays the flat wall.
layers	r_b, D_b, b_b	Bubbles for lower r_b values, viewed from the high D_b side.
varycontour1	r_b, D_b, b_b	View the wall creeping while increasing the iso-value for clipping A . So, although growing, amplitudes in the wall region do not reach the iso value, and vanish to allow looking at the dynamics for lower b_b and r_b .
majagrow	r_b, D_b, b_b	View the creeping growth of the wall with emphasising by colors of B .
cube1	r_b, D_b, s_a	Outer surface of the cubic parameter space colored by A . D_b in X, r_b in Y and s_a in Z direction. (420x420x420 voxel)
iso5_greyred	r_b, D_b, s_a	Camera orbit around the parameter cube, iso surfaces @ $A = 0.5$, colored by B .
boiling_below	r_b, D_b, s_a	View from high r_b perspective. Compare to the waves approaching the wall as in coast.mp4
7900iso08	r_b, D_b, s	Here, the diffusion values have both multiplied by 40 against the ones before. The structure sizes have been enlarged, like scaling of the equations predict. The iso surface is created at $A = 0.8$. The camera orbits around the parameter space.
redBubblesFix	r_b, D_b, s	Fixed view from high s perspective, iso surface at $A = 0.5$.

The images and videos are in the appendix file, 3d subfolder.

Conclusion

8 Too long, didn't read

With analytical techniques the bifurcation scenarios of the activator inhibitor oscillator could be displayed. There are various nonlinear phenomena including stable and unstable foci, nodes and limit cycles, partially coexisting. By using these formulas, the analytical oscillator can be driven by constant inflow/outflow of neighboring oscillators. A classification tool was built from there to analyze spacially oscillating but stationary simulation results. The transition to the synchronized temporal oscillation was explained. Behavior of dynamical solutions in larger scale 2d and 3d simulations can be understood by characterizing local oscillator states.

9 Limitation

The synchronized solutions cannot be analyzed with the method explained here. Numerical experiments, however, are the remaining chance to gain understanding.

10 Outlook

As the 2d and 3d simulations show more types of behavior than analyzed so far, more distinct parameter points should be analyzed. Especially the hysteresis is a phenomenon, which might help in oscillatory computing.

In the sense of information propagation within such a self-organized medium, may it be planar or volumetric, periodic sources at defined points could be analyzed for transfer functions to some output oscillators.

In terms of learning, anisotropic and asymmetric diffusion terms other oscillation capabilities of active media, like other ideas of Meinhardt, namely additional agents like nutrition or catalysators can be expected as useful. To put the oscillators in useful states by selecting characteristic parameters like different neuron types, this work gives a basic insight for finding good prototypes.

References

- [1] Hans Meinhardt: The algorithmic beauty of sea shells, enlarged edition. Springer 1998
- [2] OpenFoam www.openfoam.com version 2206
- [3] Paraview version 5.10.1 for visualization
- [4] python version 3.9.13: sympy, numpy, scipy, matplotlib